Chapter 1
Chiral Coupling to Magnetodipolar Radiation

Tao Yu and Gerrit E. W. Bauer

Abstract We review and extend the theory of chiral pumping of spin waves by magnetodipolar stray fields that generate unidirectional spin currents and asymmetric magnon densities. We illustrate the physical principles by two kinds of chiral excitations of magnetic films, i.e., by the evanescent Oersted field of a narrow metallic stripline with an AC current bias and a magnetic nanowire under ferromagnetic resonance.

1.1 Introduction

"Handedness" or "chirality" of wave propagation is a lively research topic in optics, acoustics, and condensed matter physics. The "spin" of magnons is rooted in the time-reversal symmetry breaking of the magnetic order and leads to chiral coupling with other excitations when locked to the momentum. This phenomenon is governed by non-universal selection rules. This Chapter clarifies a specific mechanism, viz. evanescent microwaves that can efficiently generate chiral dynamics.

Magnonics and magnon spintronics [1, 2, 3, 4] are emergent fields that hold the promise of a next-generation low-power and scalable information processing and communication technology. The generation of coherent and propagating spin waves is a crucial ingredient, which can be realized by magnetic fields generated by microwave antennas such as current-biased metallic striplines. In order to generate

Tao Yu

Max Planck Institute for the Structure and Dynamics of Matter, Luruper Chaussee 149, 22761 Hamburg, Germany, e-mail: `tao.yu@mpsd.mpg.de`

Gerrit E. W. Bauer

Institute for Materials Research & WPI-AIMR & CSRN, Tohoku University, Sendai 980-8577, Japan,
Kavli Institute of NanoScience, Delft University of Technology, 2628 CJ Delft, The Netherlands, e-mail: `G.E.W.Bauer@tudelft.nl`

stray fields with high-momentum Fourier components these must be small in size and placed close to the magnetic medium. Not only the amplitude, but also the direction of the excited spin waves depend on the excitation conditions that obey right-hand rules and are therefore *chiral*.

In this Chapter, we focus on the chirality of the dipolar coupling between the magnetization dynamics in ferromagnetic heterostructures [5, 6, 7, 8, 9, 10], while those in optics [11, 12, 13, 14, 15, 16, 17], plasmonics [18, 19], and magnetic structures with Dzyaloshinskii-Moriya interaction are treated in other chapters. We focus on the favorite material of magnonics, viz. the ferrimagnetic insulator yttrium iron garnet (YIG) with high Curie temperature and outstanding magnetic and acoustic quality [20]. Its magnons can be excited electrically by heavy metal contacts [21], acoustically [22], as well as by a large spectrum of electromagnetic waves from gigahertz (microwaves) to petahertz (light). Magnonic transducers with spatially separated contact that excite and detect magnons [5, 21, 23, 24, 25, 26, 27, 28, 29] are sensitive probes to study magnon transport. We illustrate the chiral physics for thin YIG films with in-plane magnetizations, but other materials and configurations can be treated by changing the model parameters.

The spin waves of in-plane magnetized films can be classified by the interaction that governs their dispersion as a function of wave vector, into the dipolar, dipolar-exchange and exchange type with energies ranging from a few gigahertz to many terahertz [1, 2, 3, 4, 23]. The long-wavelength modes are dipolar, whereas the short-wavelength ones are exchange. Bulk volume modes and surface (Damon-Eshbach) modes propagate along or perpendicular to the magnetization direction with different dispersion relations [30, 31, 32, 33]. Moreover, the surface modes are chiral: their propagation direction (linear momentum) is fixed by the outer product of surface normal and magnetization direction, allowing unidirectional spin current generation by dominantly exciting one surface of a magnetic film [34, 35, 36, 37]. However, Damon-Eshbach spin waves are not well suited for applications — their group velocity tends to be zero when the linear momentum is larger than the inverse of film thickness, leading to a small spin conductivity. They are also very sensitive to dephasing by surface roughness [38], and do not exist in sufficiently thin films.

An alternative to intrinsically chiral spin waves is the chiral excitation of non-chiral ones. Micromagnetic simulations [5] revealed that the AC dipolar field emitted by a magnetic nanowire on top of an in-plane magnetized film with magnetization normal to the wire can excite unidirectional spin waves. We have been motivated by experiments on an array of magnetic nanowires on top of an ultrathin YIG film that generated unidirectional spin waves parallel to the surface and perpendicular to the nanowires [7] to develop a general theory of coherent and incoherent chiral excitation of magnons [6, 8] by the dipolar interaction between the dynamics of a magnetic film and a magnetic transducer. The chirality can be traced to the different stray fields generated by spin waves with opposite polarization and propagation. By angular momentum conservation electromagnetic waves with particular polarization emitted by a magnetic transducer couple only the circularly polarized component of a spin wave with a certain propagation direction [11]. When dipolar or crystal anisotropy mixes the right and left circularly polarized components, magnons are still excited

preferentially, but not exclusively, in one direction. Finally, a (short-range) exchange coupling between film and transducer is not sensitive to the propagation direction, and reduces the chirality.

Recently, two remarkable experiments confirmed our predictions. By NV magnetometry Bertelli et al. [39] observed chiral pumping of spin waves by a stripline antenna. Wang et al. [40] measured unidirectional microwave transmission mediated by two magnetic wires on top of a thin magnetic film, i.e. chiral magnon-magnon coupling.

The chiral coupling to spin waves enables the generation and control of spin currents [6, 7, 8] or spin accumulations [9, 10] in ferromagnetic insulators, which is beneficial for spintronic devices. In this short review, we comprehensively illustrate two kinds of chiral coupling to the magneto-dipolar radiation, including the evanescent field of a thin stripline that carries an AC current (Sec. 1.2) and that of a magnetic wire under resonant excitation (Sec. 1.3).

1.2 Chiral excitation of spin waves by metallic stripline

We call a wave "chiral" when it propagates with handedness, i.e. in a certain direction that is determined by two other control vectors, such as surface normal and magnetic field. A rotating *electrical* dipole [41, 42] excites surface plasmon polaritons in one direction only [18, 19, 41], while a precessing *magnetic* dipole excite magnons unidirectionally [43, 44]. Here we analyze solutions of the combined Maxwell and Landau-Lifshitz-Gilbert equations that explain the available experimental evidence. We analyze the near microwave field from a normal metal strip line in Sec. 1.2.1 and its effect on a thin magnetic film in Sec. 1.2.2 (see Fig. 1.1). We focus for simplicity on a configuration in which the film normal is along the x-direction, $\hat{\mathbf{z}}$ is parallel to a stripline that is assumed to be very long, and the excited spin waves propagate in the y-direction.

1.2.1 Oersted magnetic fields

We first demonstrate that even though the magnetic field of a stripline is linearly-polarized in real space (see Fig. 1.1), it is chiral in momentum space. Ampere's Law states that the current density $\mathbf{J}(\mathbf{r})$ generates the vector potential [42]

$$\mathbf{A}(\mathbf{r}, t) = \frac{\mu_0}{4\pi} \int d\mathbf{r}' dt' \frac{\mathbf{J}(\mathbf{r}', t')}{|\mathbf{r} - \mathbf{r}'|} \delta\left(t' + \frac{|\mathbf{r} - \mathbf{r}'|}{c} - t\right), \tag{1.1}$$

where μ_0 is the vacuum permeability and the delta-function represents (non-relativistic) retardation. For a harmonic source $\mathbf{J}(t) \sim \mathbf{J}(\omega)e^{-i\omega t}$,
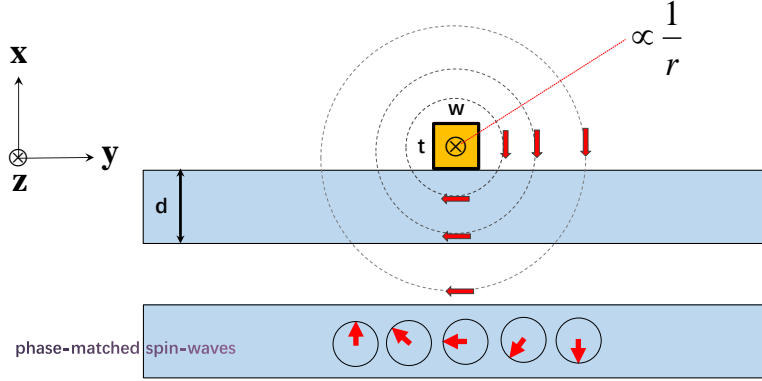
Fig. 1.1 (Color online) Chiral excitation of spin waves in a magnetic thin film by the near field of a stripline antenna. The ac magnetic field is axially symmetric with an oscillating modulus and in the film a position-dependent linear polarization. It excites spin waves with the same frequency and phase-matched spatial amplitude. The film magnetization direction (here parallel to the stripline) can be tuned by a static magnetic field.

$$\mathbf{A}(\mathbf{r}, \omega) = \frac{\mu_0}{4\pi} \int d\mathbf{r}' \mathbf{J}(\mathbf{r}', \omega) \frac{e^{ik|\mathbf{r}-\mathbf{r}'|}}{|\mathbf{r} - \mathbf{r}'|}, \tag{1.2}$$

where $k = \omega/c$. The current in the stripline is uniform over the cross section of width w and thickness t as well as length $L \ll c/\omega$. In the long wavelength limit and square cross section $\mathbf{J}(\mathbf{r}, \omega) \simeq \delta(x)\delta(y)\mathcal{J}(\omega)\hat{\mathbf{z}}$, where $\mathcal{J}$ is the total electric current, leading to

$$\mathbf{A}(\mathbf{r}, \omega) = \frac{\mu_0}{4\pi} \mathcal{J}(\omega)\hat{\mathbf{z}} \int_{-\infty}^{\infty} dz' \frac{e^{ik\sqrt{x^2+y^2+z'^2}}}{\sqrt{x^2 + y^2 + z'^2}}, \tag{1.3}$$

which does not depend on z. Substituting the Weyl identity [41]

$$\frac{e^{ik\sqrt{x^2+y^2+z^2}}}{\sqrt{x^2 + y^2 + z^2}} = \frac{i}{2\pi} \int dk_y dk_z \frac{e^{ik_x|x|+ik_y y+ik_z z}}{k_x}, \tag{1.4}$$

where $k = \sqrt{k_x^2 + k_y^2 + k_z^2}$ and $k_x = |a| + i|b|$ is complex, into Eq. (1.3) yields

$$\mathbf{A}(x, y, \omega) = \frac{i\mu_0}{4\pi} \mathcal{J}(\omega)\hat{\mathbf{z}} \int dk_y \frac{e^{ik_x|x|+ik_y y}}{k_x}. \tag{1.5}$$

The magnetic field $\mathbf{H}(\mathbf{r}) = \nabla \times \mathbf{A}(\mathbf{r})/\mu_0 = \left(\partial_y A_z, -\partial_x A_z, 0\right)/\mu_0$ is transverse to the wire, see Fig. 1.1. Below the stripline ($x < 0$),

$$H_x(x, y, \omega) \equiv \int dk_y e^{ik_y y} H_x(x, k_y) = -\int dk_y e^{ik_y y} \frac{\mathcal{J}(\omega)}{4\pi} \frac{k_y}{k_x} e^{-ik_x x},$$

$$H_y(x, y, \omega) \equiv \int dk_y e^{ik_y y} H_y(x, k_y) = -\int dk_y e^{ik_y y} \frac{\mathcal{J}(\omega)}{4\pi} e^{-ik_x x}, \qquad (1.6)$$

where $k_x = \sqrt{(\omega/c)^2 - k_y^2}$. Directly above or below the wire $H_x(x, y = 0, \omega) = 0$, i.e. the magnetic field is linearly-polarized along y. The polarization rotates as a function of y until $H_y(0, y \to \infty, \omega) = 0$. Surprisingly, a circular polarization emerges in the Fourier components

$$H_x(x, k_y, \omega) = -\frac{\mathcal{J}(\omega)}{4\pi} \frac{k_y}{k_x} e^{-ik_x x},$$

$$H_y(x, k_y, \omega) = -\frac{\mathcal{J}(\omega)}{4\pi} e^{-ik_x x}. \qquad (1.7)$$

For an evanescent field with $k_y > \omega/c \equiv k$, $k_x = i\sqrt{k_y^2 - k^2}$ and $x < 0$

$$H_x(x, k_y, \omega) = \frac{i\mathcal{J}(\omega)}{4\pi} \frac{k_y}{\sqrt{k_y^2 - k^2}} e^{\sqrt{k_y^2 - k^2}x},$$

$$H_y(x, k_y, \omega) = -\frac{\mathcal{J}(\omega)}{4\pi} e^{\sqrt{k_y^2 - k^2}x}. \qquad (1.8)$$

At microwave frequencies $\omega/(2\pi) \sim 10$ GHz, $k \equiv \omega/c \sim 200$ m^{-1} and wavelength $\lambda = 2\pi/k \sim 3$ cm. The spin wavelength at the same frequency is much smaller with $\sqrt{k_y^2 + k_z^2} \gg \omega/c$, so we are in the near-field limit. The magnetic field component $H_x \to i\,\mathrm{sgn}(k_y)H_y$ is then circularly polarized with a sign locked to its linear momentum.

For a finite rectangular cross section with $0 < x < t$ and $-w/2 < y < w/2$ the Fourier components of the magnetic field read

$$H_x(x, k_y, \omega) = i\frac{J(\omega)}{4\pi} \mathcal{F}(t, w) \frac{k_y}{\sqrt{k_y^2 - k^2}} e^{\sqrt{k_y^2 - k^2}x},$$

$$H_y(x, k_y, \omega) = -\frac{J(\omega)}{4\pi} \mathcal{F}(t, w) e^{\sqrt{k_y^2 - k^2}x}, \qquad (1.9)$$

which differ from the previous results only by the form factor

$$\mathcal{F}(t, w) = \frac{4}{k_x k_y} e^{ik_x \frac{t}{2}} \sin\left(k_x \frac{t}{2}\right) \sin\left(k_y \frac{w}{2}\right). \qquad (1.10)$$

Irrespective to the shape of the stripline, the magnetic field components are circularly polarized when $|k_y| \gg \omega/c$ but oscillate now as function of the wave vector.

1.2.2 Chiral excitation of spin waves

We focus here on thin YIG films with thickness $d \sim O(10\,\text{nm})$, which allows an analytical treatment of the dispersion and spin wave amplitudes in the dipolar-exchange regime [6]. An applied magnetic field $H_{\text{app}}\hat{\mathbf{z}}$ parallel to the stripline corresponds to the Damon-Eshbach configuration, but we stress that for ultrathin films there are no Damon-Eshbach surface modes. The spin wave energy dispersion [6]

$$\omega_{\mathbf{k}} = \mu_0 \gamma M_s \sqrt{\left[\Omega_H + \alpha_{\text{ex}} k^2 + 1 - f(|k_y|)\right]\left[\Omega_H + \alpha_{\text{ex}} k^2 + (k_y^2/k^2) f(|k_y|)\right]}, \tag{1.11}$$

where $-\gamma$ is the electron gyromagnetic ratio, M_s denotes the saturated magnetization, α_{ex} is the exchange stiffness, $\Omega_H \equiv H_{\text{app}}/M_s$, and

$$f(|k_y|) = 1 - \frac{1}{|k_y|d} + \frac{1}{|k_y|d}\exp(-|k_y|d), \tag{1.12}$$

is highly anisotropic. The spin waves amplitudes across sufficiently thin films are constant [6]:

$$m_x = \sqrt{\frac{B+1}{4d(B-1)}}, \qquad m_y = i\sqrt{\frac{B-1}{4d(B+1)}}, \tag{1.13}$$

where we chose the normalization [45, 46, 38]

$$\int d\mathbf{r}\left[m_x(\mathbf{r})m_y^*(\mathbf{r}) - m_x^*(\mathbf{r})m_y(\mathbf{r})\right] = -i/2, \tag{1.14}$$

and

$$B = \frac{1/2 - (1/2)\left(1 + k_y^2/k^2\right)f(|k_y|)}{\omega_{\mathbf{k}}/(\mu_0 \gamma M_s) - \left(\Omega_H + \alpha_{\text{ex}}k_y^2 + 1/2\right) + (1/2)\left(1 - k_y^2/k^2\right)f(|k_y|)}. \tag{1.15}$$

When $k_y \to 0$: $f(|k_y|) = 0$, $\lim_{k_y \to 0}\omega_{\mathbf{k}} = \mu_0 \gamma M_s\sqrt{\Omega_H(\Omega_H + 1)}$, $B \to -1 - 2\Omega_H - 2\sqrt{\Omega_H(\Omega_H + 1)}$. When $\Omega_H \to 0$ with a small static magnetic field, $B \to -1 - 2\sqrt{\Omega_H}$, $|m_y| \gg |m_x|$, so the Kittel mode is (nearly) linearly polarized. In the opposite (exchange) limit of $|k_y|d \gg 1$ and $\alpha_{\text{ex}}k^2 \gg 1$, $f(k_y) \to 1$, $|B| \gg 1$, and the spin waves are right-circularly polarized with $m_y = im_x$.

The Oersted magnetic fields from the stripline interact with spin waves by the Zeeman interaction [47]

$$\hat{H}_{\text{int}} = -\mu_0 \int \mathbf{M}(\mathbf{r}) \cdot \mathbf{H}(\mathbf{r})dV. \tag{1.16}$$

The excited magnetization in the film can be expressed by time-dependent perturbation theory [48]

$$M_\alpha(x, \boldsymbol{\rho}, t) = -i \int_{-\infty}^{t} dt' \left\langle \left[\hat{\mathbf{M}}_\alpha(x, \boldsymbol{\rho}, t), \hat{H}_{\mathrm{int}}(t') \right] \right\rangle. \qquad (1.17)$$

in terms of the retarded spin susceptibility tensor

$$\chi_{\alpha\delta}(x, x'; \boldsymbol{\rho} - \boldsymbol{\rho}'; t - t') = i\Theta(t - t') \left\langle \left[\hat{\mathbf{S}}_\alpha(x, \boldsymbol{\rho}, t), \hat{\mathbf{S}}_\delta(x', \boldsymbol{\rho}', t') \right] \right\rangle, \qquad (1.18)$$

where $\hat{\mathbf{S}}_\alpha = -\hat{\mathbf{M}}_\alpha/(\gamma\hbar)$ is the spin operator and a sum over repeated indices is implied. Hence [6, 7, 8],

$$\mathbf{M}_\alpha(x, k_y, \omega) = \mu_0 (\gamma\hbar)^2 \int_{-d}^{0} dx' \chi_{\alpha\beta}(x, x', k_y, \omega) H_\beta(x', k_y, \omega), \qquad (1.19)$$

where

$$\chi_{\alpha\beta}(x, x', \mathbf{k}, \omega) = -\frac{2M_s}{\gamma\hbar} m_\alpha^{(\mathbf{k})}(x) m_\beta^{(\mathbf{k})*}(x') \frac{1}{\omega - \omega_{\mathbf{k}} + i\Gamma_{\mathbf{k}}}. \qquad (1.20)$$

Here, $\Gamma_{\mathbf{k}} = 2\alpha\omega_{\mathbf{k}}$ is the reciprocal lifetime in terms of the Gilbert damping constant α. The excitation efficiency is determined by $m_\beta^{(k_y)*}(x') H_\beta(x', k_y, \omega)$, so the excitation of circularly polarized spin waves is chiral (or unidirectional) by the polarization-momentum locking with the stripline magnetic field. Since the amplitudes across thin films are constant for $kd \ll 1$, the excited magnetization in time domain and position space is the real part of the inverse Fourier transform ($q \equiv k_y$),

$$\mathbf{M}_\alpha(x, y, t) = \sum_q e^{iqy - i\omega t} \mathbf{M}_\alpha(x, q)$$

$$\approx 2i\mu_0 \gamma\hbar d M_s m_\alpha^{(q_\omega)} m_\beta^{(q_\omega)*} \frac{1}{v_{q_\omega}} e^{-i\omega t} \begin{cases} e^{iq_\omega y - \delta_\omega y} H_\beta(q_\omega, \omega) & \text{for } y > 0 \\ e^{-iq_\omega y + \delta_\omega y} H_\beta(-q_\omega, \omega) & y < 0 \end{cases}, \qquad (1.21)$$

where $q_\omega + i\delta_\omega$ is the positive root of $\omega_q = \omega + i\Gamma_q$, and v_{q_ω} is the modulus of the group velocity $|\partial\omega_q/\partial q|_{q_\omega}$. The polarization-momentum locking of the stripline field generates two different magnetization dynamics. When the excited spin waves are circularly polarized, they not only propagate in one direction only, but the excitation is also spatially limited to half of the film, i.e. the chirality is perfect. We can understand this phenomenon in terms of the interference between the spin waves and the stripline magnetic field that is constructive and destructive on opposite sides, as illustrated in Fig. 1.1.

The dominant excitation direction can be switched with the film magnetization. For a finite angle θ between the saturated magnetization and the stripline, the situation becomes complicated by the reduced symmetry. It is advantageous to transform Eq. (1.21) following the Supplements of Refs. [7, 8]:

$$m_x^{(k_y)} \to m_x^{(\mathbf{l})}, \quad m_y^{(k_y)} \to \cos\theta m_y^{(\mathbf{l})}$$

where $\mathbf{l} = (0, q\cos\theta, q\sin\theta)$ and q is determined by $\omega_{\mathbf{l}} + i2\alpha\omega_{\mathbf{l}} = \omega$. Even for circularly polarized spin waves, the chirality is not perfect anymore while situation is complicated for elliptical spin waves since their polarization depends on the wave vector. For $\theta_c = \pi/2$ the chirality always vanishes. Since mirror symmetry is broken, the two roots $\left| q_\omega^{(+)} + i\delta_\omega^{(+)} \right| \neq \left| -q_\omega^{(-)} - i\delta_\omega^{(-)} \right|$ for $\theta \neq 0, \theta_c$. The wavelength and propagation direction of the excited spin waves may therefore be different on the two sides of the stripline.

Figure 1.2 is a plot of the calculated excited magnetization profile for a YIG magnetic film for constant current density but different excitation frequencies $\omega/(2\pi)$. At low frequencies the excitation efficiency is high, but since the dipolar interaction
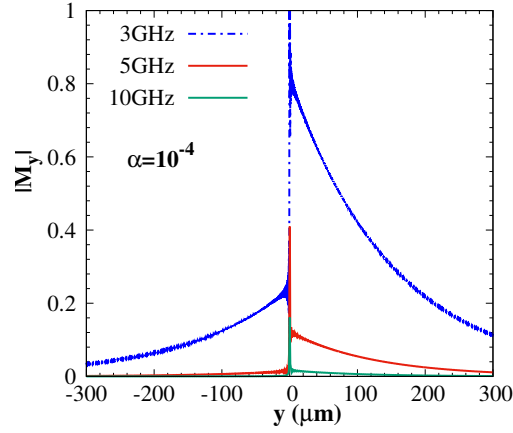

Fig. 1.2 Calculated magnetization amplitude profile $\left| M_y(y) \right|$ of a YIG film with ground state magnetization along z, $d = 20$ nm, and $\alpha = 10^{-4}$, excited by a metal stripline with $t = 100$ nm, $w = 1$ μm, carrying an AC current with excitation frequencies $\omega/(2\pi) = 3$, 5, and 10 GHz. $\left| M_y(y) \right|$ is proportional to the current density, which is here normalized by its maximum value for $\omega/(2\pi) = 3$ GHz.

renders the spin wave precession elliptical, the chirality is relatively weak. At high frequencies the chirality improves, but the magnetization amplitude is suppressed by the form factor $\sin(k_y w/2)$ that favors spin waves with wavelengths around w. A narrower stripline helps to excite spin waves with short wavelengths and higher chirality. The spatial decay on both sides of the stripline is governed by the Gilbert damping. Chiral spin waves can also be generated by magnetic striplines with high coercivity that allow efficient excitation and almost perfect chirality at frequencies > 10 GHz. The physics is quite different, however, and explained in the following section.

1.3 Chiral spin wave excitation and absorption by a magnetic transducer

Coherent exchange-dipolar spin waves with short wavelengths $\lambda < 100$ nm are attractive information carriers by their long lifetime and high group velocity. According to the discussion above their excitation is difficult because striplines cannot be fabricated much finer than this wave length. A small stripline cross section also increases Joule heating and thereby limits the maximum applicable currents. A new strategy is to use magnetic nanowires with high coercivity and resonance frequencies that can be fabricated with the same feature sizes as normal metal ones. Rather than applying an AC current directly, magnetic nanowires can be used as "antennas" that are excited by proximity coplanar wave guides [5, 25, 26, 27, 28, 29]. A direct contact between film and nanowires can suppress chirality by the interface exchange interaction and associated spin transfer [6], but an insulating spacer of a few atomic monolayers strongly suppresses exchange without much affecting the dipolar interaction. Figure1.3 shows a typical configuration with a Co nanowire on top of the YIG film.
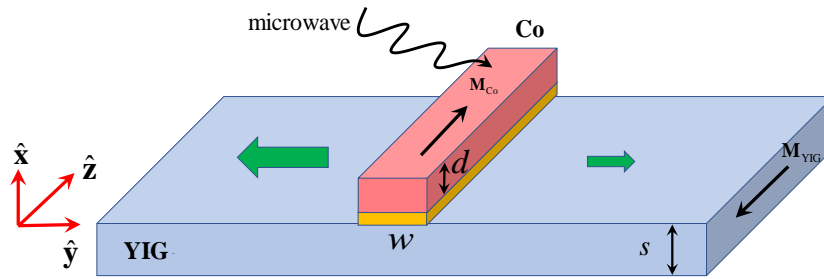

Fig. 1.3 A magnetic (Co) nanowire transducer separated by a non-magnetic spacer (optional) from a YIG film. The dipolar coupling is maximized for the antiparallel magnetization. The direction of the magnon spin currents pumped into the $\pm\hat{\mathbf{y}}$-directions is indicated by the green arrows, whose size indicates the magnitude of the magnon currents. The black arrows indicate the (nearly uniform) microwave input to the magnetic nanowire.

1.3.1 Chiral magnetodipolar field

The dipolar field from the magnetic nanowire fundamentally differs from the Oersted field of the AC current-biased normal metal wire discussed above. The precessing magnetization is a magnetic dipole and generates a rotating dipolar field rather than

the oscillating axially symmetric field of the normal metal wire sketched in Fig. 1.1. The amplitudes of dipolar waves decay faster than that of (monopolar) current-induced ones, but are still long-ranged compared to e.g. the exchange interaction. The nanowire and its equilibrium magnetization are parallel to the z-direction as shown in Fig. 1.3. When driven with a frequency ω, the macrospin (Kittel) magnetization dynamics of a wire with thickness d and width w is the real part of

$$\tilde{M}_{x,y}(\mathbf{r},t) = \tilde{m}_{x,y}\Theta(x)\Theta(-x+d)\Theta(y+w/2)\Theta(-y+w/2)e^{-i\omega t}, \qquad (1.22)$$

where $\Theta(x)$ is the Heaviside step function and $\tilde{m}_{x,y}$ are constant amplitudes that depend on the geometry and the excitation power. The corresponding dipolar magnetic field [47]

$$\tilde{h}_\beta(\mathbf{r},t) = \frac{1}{4\pi}\partial_\beta\partial_\alpha \int \frac{\tilde{M}_\alpha(\mathbf{r}',t)}{|\mathbf{r}-\mathbf{r}'|}d\mathbf{r}'$$

$$= \frac{1}{4\pi}\partial_\beta\partial_\alpha \int dz' \int_0^d dx' \int_{-\frac{w}{2}}^{\frac{w}{2}} dy' \frac{\tilde{m}_\alpha e^{-i\omega t}}{\sqrt{z'^2 + (x-x')^2 + (y-y')^2}}. \quad (1.23)$$

We use the Coulomb integral [6, 41]

$$\frac{1}{\sqrt{z'^2 + (x-x')^2 + (y-y')^2}} = \frac{1}{2\pi} \int dk_x dk_y \frac{e^{-|z'|\sqrt{k_x^2+k_y^2}}}{\sqrt{k_x^2 + k_y^2}} e^{ik_x(x-x')+ik_y(y-y')},$$

$$(1.24)$$

a variation of the Weyl identity used in Eq. (1.4), to express the magnetic field below the nanowire ($x < 0$) with partial Fourier components k_y

$$\tilde{h}_\beta(k_y,x,t) = \int h_\beta(\mathbf{r},t)e^{-ik_y y}dy$$

$$= \frac{1}{\pi} \int dk_x(k_x\tilde{m}_x + k_y\tilde{m}_y)k_\beta e^{ik_x x - i\omega t} \frac{1}{k_x^2 + k_y^2} \frac{1 - e^{-ik_x d}}{ik_x} \frac{\sin(k_y w/2)}{k_y}.$$

$$(1.25)$$

Closing the contour of the k_x integral in the lower half of the complex plane yields

$$\begin{pmatrix} \tilde{h}_x(k_y,x,t) \\ \tilde{h}_y(k_y,x,t) \end{pmatrix} = -\frac{i}{4\pi}e^{|k_y|x}(1 - e^{-|k_y|d})\frac{2\sin(k_y w/2)}{k_y|k_y|} \begin{pmatrix} |k_y| & ik_y \\ ik_y & -|k_y| \end{pmatrix} \begin{pmatrix} \tilde{m}_x \\ \tilde{m}_y \end{pmatrix} e^{-i\omega t}.$$

$$(1.26)$$

The perfectly right-circularly polarized wire dynamics of the Kittel mode in rectangular wires ($\tilde{m}_y = i\tilde{m}_x$ when $w = d$) implies that the Fourier components of $\tilde{\mathbf{h}}$ with $k_y > 0$ vanish. The Fourier component with $k_y < 0$ is then perfectly left circularly polarized $(\tilde{h}_y = -i\tilde{h}_x)$. Above the nanowire, the magnetic field direction and polarization are reversed, as sketched in Fig. 1.4. The elliptical polarization of the Kittel mode in rectangular nanowires breaks the perfect chirality. Analogous expressions can be derived for arbitrarily shaped magnetic transducers such as discs,

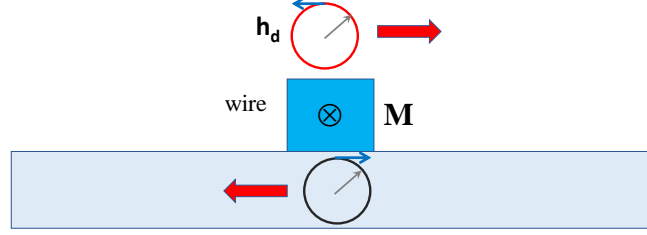but analytical expressions become complex or may not exist when the symmetry is reduced.

Fig. 1.4 Dipolar magnetic field $\tilde{\mathbf{h}}$ generated by a Kittel mode excitation of a magnetic nanowire ($\parallel \hat{\mathbf{z}}$). The thick red and thin blue arrows indicate the propagation and precession directions of $\tilde{\mathbf{h}}$, respecctively, both above and below the wire.

Equation (1.21) can be used also for magnetic fields $\tilde{\mathbf{h}}$ generated by a magnetic transducer, i.e. Eq. (1.26), a left-circularly polarized dipolar field that propagates to the left. An ellipticity of the spin waves in the film does not affect the chirality since the excited magnetization still propagates to the left and lives only in the left half-space, but it reduces the excitation efficiency. The same holds when the Kittel mode in a rectangular nanowire is elliptical and the spin waves in the film are circularly polarized. We illustrate these conclusion below from different viewpoint.

Let us compare the dipolar stray fields $\tilde{\mathbf{h}}$ emitted by the excited magnetic wire and $\mathbf{H}$ generated by a stripline as discussed in the previous section. The main difference between these "Oersted" vs. "dipolar" radiation is that the latter has additional chirality that induces a circularly-polarized magnetic field in real space, in contrast to the linearly-polarized magnetic field of the former. Equation (1.26) can be summarized as $\tilde{h}_x \propto |k_y|(\tilde{m}_x + i\,\text{sgn}(k_y)\tilde{m}_y)$ and $\tilde{h}_y \propto ik_y(\tilde{m}_x + i\,\text{sgn}(k_y)\tilde{m}_y)$. $\tilde{h}_y = i\,\text{sgn}(k_y)\tilde{h}_x$ is the polarization-momentum locking in reciprocal space, which is the same as that of the evanescent Oersted field. However, the magnetic chirality affects $\tilde{m}_x + i\,\text{sgn}(k_y)\tilde{m}_y$: for right circularly-polarized (when $w = d$) $\tilde{m}_y = i\tilde{m}_x$, $\tilde{\mathbf{h}}$ simply vanishes for positive k_y. Thus, the magnetic field is unidirectional with linear momentum components normal to the wire that are negative, which is more than just a locking between polarization and momentum. $\tilde{\mathbf{h}}$ therefore couples chirally to spins with arbitrary polarizations.

The Zeeman interaction $\sim \mathbf{M} \cdot \tilde{\mathbf{H}}$ between the wire and film is governed as used above is completely equivalent to the interaction $\sim \tilde{\mathbf{M}} \cdot \mathbf{h}$, where $\tilde{\mathbf{M}}$ is the wire magnetization and $\mathbf{h}$ the dipolar field generated by the spin waves in the film. It is instructive to discuss the physics from this second viewpoint. We assume again that the equilibrium wire magnetization is fixed by the form anisotropy to the z-direction. A sufficiently soft film magnetization can be rotated in the x-z plane by an applied magnetic field, but we address here only (anti)parallel magnetizations but general wave propagation direction [7, 8]. We allow for the elliptical spin wave polarization in the magnetostatic regime. At frequency ω and in the coordinate

system defined in Fig. 1.3 with in-plane wave vector $\mathbf{k} = k_y \hat{\mathbf{y}} + k_z \hat{\mathbf{z}}$, we define $M_x(\mathbf{r}, t) = m_R^{(\mathbf{k})}(x) \cos(\mathbf{k} \cdot \boldsymbol{\rho} - \omega t)$ and $M_y(\mathbf{r}, t) \equiv -m_R^{(\mathbf{k})}(x) \sin(\mathbf{k} \cdot \boldsymbol{\rho} - \omega t)$, where $m_R^{(\mathbf{k})}(x)$ is the time-independent amplitude into the film and $\boldsymbol{\rho} = y\hat{\mathbf{y}} + z\hat{\mathbf{z}}$. The dipolar field outside the film with $\alpha, \beta = \{x, y, z\}$ [47],

$$h_\beta(\mathbf{r}, t) = \frac{1}{4\pi} \partial_\beta \partial_\alpha \int d\mathbf{r}' \frac{M_\alpha(\mathbf{r}', t)}{|\mathbf{r} - \mathbf{r}'|}, \qquad (1.27)$$

then reads

$$\begin{pmatrix} h_x(\mathbf{r}, t) \\ h_y(\mathbf{r}, t) \\ h_z(\mathbf{r}, t) \end{pmatrix} = \begin{pmatrix} \left(k + \eta k_y\right) \cos\left(\mathbf{k} \cdot \boldsymbol{\rho} - \omega t\right) \\ \left(\frac{k_y^2}{k} + \eta k_y\right) \sin\left(\mathbf{k} \cdot \boldsymbol{\rho} - \omega t\right) \\ k_z \left(\frac{k_y}{k} + \eta\right) \sin\left(\mathbf{k} \cdot \boldsymbol{\rho} - \omega t\right) \end{pmatrix} \frac{1}{2} e^{-\eta k x} \int dx' m_R^{\mathbf{k}}(x') e^{\eta k x'}, \quad (1.28)$$

where $x > 0$ ($x < -s$) indicates the dipolar field above (below) the film, $\eta = 1$ (-1) when $x > 0$ ($x < -s$), $k = |\mathbf{k}|$, and the spatial integral is over the film thickness.

When $k_z = 0$, $k_y \neq 0$ spin waves propagate normal to the wire and $h_z = 0$. The distribution of the dipolar field above and below the film then strongly depends on the sign of k_y: the dipolar field generated by the right (left) moving spin waves only appears above (beneath) the film [6, 7, 8] and precesses in the opposite direction of the magnetization. These features provide an alternative explanation of the chiral coupling between these spin waves and *any* magnet close to the film surface [6, 7]. The chiral dipolar coupling is most pronounced when the magnetizations of the film and wire are antiparallel [6, 7, 8].

When the film magnetization is rotated by 90 degrees in perpendicular to the wire, the wire magnetization excites spin waves that propagate *parallel* to the magnetization ($k_y = 0$, $h_y = 0$), which for thick films correspond to the backward moving bulk modes. Surprisingly, these also couple chirally to the wire dynamics, but by a different mechanism. According to Eq. (1.4), $h_x \propto |k_z| \cos(k_z z - \omega t)$ and $h_z \propto \eta k_z \sin(k_z z - \omega t)$. The dipolar fields generated by spin waves with positive (negative) k_z are left (right) circularly polarized, respectively, while below the film, the polarizations are reversed. These spin waves chirally interact with the transducer magnet since the polarization of the transverse magnetization dynamics of the latter has to match that of the stray field $\mathbf{h}$ [5].

Therefore, two mechanisms contribute to the chiral excitation, depending on the magnetic configuration. When spin waves propagate perpendicular to the magnetization with opposite momenta, their dipolar fields vanish on opposite sides of the film; when propagating parallel to the magnetization, their dipolar field is chiral, i.e., polarization-momentum locked. Purely chiral coupling between magnons can be achieved in the former case without constraints on the polarization of the local magnet, but in the latter case elliptical polarization of the wire leads to partial chirality.

The resonance frequency of a magnetic nanowire can be tuned by an applied magnetic field and excites spin waves in a frequency window that is governed by the

wire form factor. The magnetodipolar field emitted by a coherently excited magnetic nanowire array can also be chiral [6, 7]. However, such a nanowire grating with period a and translational symmetry $na\hat{\mathbf{y}}$ excites discrete spin waves with momenta $(m\pi/a)\hat{\mathbf{y}}$, where $\{m, n\} \in Z_0$ that are observable as sharp and intense feature in the microwave transmission (more details are shown below).

1.3.2 Non-local detection

Here we illustrate the principle of non-local excitation and detection of magnons by a device consisting of two magnetic nanowires on top of a YIG film. The generation of DC currents by AC forces in the absence of a DC bias is generally referred to as "pumping" [49]. Spin pumping is the injection of a spin current by the magnetization dynamics of a magnet into a normal metal contact by the interface exchange interaction [50, 51]. *Chiral spin pumping* is the generation of unidirectional spin waves by the dynamics of a proximity magnetic wire as discussed above. Its inverse is the *chiral spin absorption,* i.e. the wire dynamics induced by the stray fields caused by spin waves in the film. We develop below a semi-analytic theory of chiral spin pumping/absorption for antiparallel magnetic configurations and describe two effects — non-reciprocal microwave transmission and chiral spin Seebeck effect. Whereas the former is due to coherent pumping by applied microwaves, the latter represents the incoherent (thermal) pumping by a temperature difference [59, 60, 61, 62]. Both effects can be observed in terms of the magnon population or temperature in the detector, e.g., inductively or by light scattering.

We switch from a purely classical picture of previous sections to a quantum description of the chiral coupling in terms of Hamiltonian matrix elements between generalized harmonic oscillators. This does not introduce new physics since we can simply replace operators by classical amplitudes, but it provides a compact formalism used in many other fields such as nanomechanical systems and optics, and prepares the stage for the treatment of real quantum problems. For simplicity, we focus on the antiparallel magnetic configuration with maximized dipolar coupling (for arbitrary magnetization directions see [8]). The dipolar coupling of the wire magnetization $\tilde{\mathbf{M}}$ with that of a film $\mathbf{M}$ is governed by the Zeeman interaction with the respective stray magnetic fields $\mathbf{h}$ and $\tilde{\mathbf{h}}$ [47]

$$\hat{H}_{\text{int}}/\mu_0 = -\int \tilde{\mathbf{M}}(\mathbf{r}, t) \cdot \mathbf{h}(\mathbf{r}, t) d\mathbf{r} = -\int \mathbf{M}(\mathbf{r}, t) \cdot \tilde{\mathbf{h}}(\mathbf{r}, t) d\mathbf{r}, \qquad (1.29)$$

where $\mathbf{h}$ and $\tilde{\mathbf{h}}$ have been introduced in Eqs. (1.28) and (1.26). The magnetization dynamics of film ($\hat{\mathbf{M}}$) and nanowire ($\hat{\tilde{\mathbf{M}}}$) are now interpreted as operators with Cartesian components $\beta \in \{x, y\}$. To leading order of the expansion in magnon creation and annihilation operators [45, 46, 38],

$$\hat{M}_{\beta}(\mathbf{r}) = -\sqrt{2M_s\gamma\hbar} \sum_{\mathbf{k}} \left[m_{\beta}^{(\mathbf{k})}(x) e^{i\mathbf{k}\cdot\boldsymbol{\rho}} \hat{\alpha}_{\mathbf{k}} + \mathrm{H.c.} \right],$$

$$\hat{\tilde{M}}_{\beta}(\mathbf{r}) = -\sqrt{2\tilde{M}_s\gamma\hbar} \sum_{k_z} \left[\tilde{m}_{\beta}^{(k_z)}(x,y) e^{ik_z z} \hat{\beta}_{k_z} + \mathrm{H.c.} \right], \tag{1.30}$$

where M_s and $\tilde{M}_s$ are the respective saturation magnetizations, $m_{\beta}^{(\mathbf{k})}(x)$ and $\tilde{m}_{\beta}^{(k_z)}(x,y)$ are the spin wave amplitudes across the film and nanowire, and $\hat{\alpha}_{\mathbf{k}}$ and $\hat{\beta}_{k_z}$ denote the magnon (annihilation) operator in the film and nanowire, respectively. The total system Hamiltonian then reads

$$\hat{H}/\hbar = \sum_{\mathbf{k}} \omega_{\mathbf{k}} \hat{\alpha}_{\mathbf{k}}^{\dagger} \hat{\alpha}_{\mathbf{k}} + \sum_{k_z} \tilde{\omega}_{k_z} \hat{\beta}_{k_z}^{\dagger} \hat{\beta}_{k_z}$$

$$+ \sum_{\mathbf{k}} \left(g_{\mathbf{k}} e^{-ik_y y_0} \hat{\alpha}_{\mathbf{k}}^{\dagger} \hat{\beta}_{k_z} + g_{\mathbf{k}}^* e^{ik_y y_0} \hat{\beta}_{k_z}^{\dagger} \hat{\alpha}_{\mathbf{k}} \right), \tag{1.31}$$

where $\omega_{\mathbf{k}}$ and $\tilde{\omega}_{k_z}$ are the frequencies of spin waves in the film and nanowire and the coupling

$$g_{\mathbf{k}} = F(\mathbf{k}) \left(m_x^{(\mathbf{k})*}, m_y^{(\mathbf{k})*} \right) \begin{pmatrix} |\mathbf{k}| & ik_y \\ ik_y & -k_y^2/|\mathbf{k}| \end{pmatrix} \begin{pmatrix} \tilde{m}_x^{(k_z)} \\ \tilde{m}_y^{(k_z)} \end{pmatrix}, \tag{1.32}$$

with $F(\mathbf{k}) = -\mu_0\gamma\sqrt{M_s\tilde{M}_s/L}\phi(\mathbf{k})$. The form factor $\phi(\mathbf{k}) = 2\sin(k_y w/2)(1 - e^{-kd})(1 - e^{-ks})/(k_y k^2)$ couples spin waves with wavelengths of the order of the nanowire width (mode selection) and $\lim_{\mathbf{k}\to 0} \phi(\mathbf{k}) = wsd$. Pure exchange waves are right-circularly polarized with $m_y^{(k_y)} = im_x^{(k_y)}$ and their coupling is perfectly chiral since $g_{-|k_y|} = 0$ and $g_{|k_y|} \neq 0$.

Eqs. (1.11) and (1.13) give the spin-wave dispersion and amplitudes in the thin film. The spin waves propagate in the nanowire along $\hat{\mathbf{z}}$ with amplitudes [6, 8]

$$\tilde{m}_x^{k_z} = \sqrt{\frac{1}{4\mathcal{D}(k_z)wd}}, \quad \tilde{m}_y^{k_z} = i\sqrt{\frac{\mathcal{D}(k_z)}{4wd}}, \tag{1.33}$$

where

$$\mathcal{D}(k_z) = \sqrt{\frac{H_{\mathrm{app}} + N_{xx}\tilde{M}_s + \tilde{\lambda}_{\mathrm{ex}}k_z^2\tilde{M}_s}{H_{\mathrm{app}} + N_{yy}\tilde{M}_s + \tilde{\lambda}_{\mathrm{ex}}k_z^2\tilde{M}_s}}. \tag{1.34}$$

H_{app} and $\tilde{\lambda}_{\mathrm{ex}}$ are the applied magnetic field and the exchange stiffness of the nanowire, respectively. The demagnetization factors $N_{xx} \simeq w/(d+w)$ and $N_{yy} = d/(d+w)$ [6] also govern the spin waves frequency

$$\tilde{\omega}_{k_z} = \mu_0\gamma\sqrt{(H_{\mathrm{app}} + N_{yy}\tilde{M}_s + \tilde{\lambda}_{\mathrm{ex}}k_z^2\tilde{M}_s)(H_{\mathrm{app}} + N_{xx}\tilde{M}_s + \tilde{\lambda}_{\mathrm{ex}}k_z^2\tilde{M}_s)}. \tag{1.35}$$

When the magnetic field is antiparallel to the nanowire magnetization we require $|H_{app}| < \min\{N_{yy}\tilde{M}_s, N_{xx}\tilde{M}_s\}$. The ellipticity of the Kittel mode with $k_z = 0$ is strongly affected by the shape anisotropy when the applied field is sufficiently small and the aspect ratio large: when $d \ll w$, $N_{xx} \rightarrow 1$, $N_{yy} \rightarrow 0$, $\mathcal{D}$ is large and the mode is nearly linearly-polarized. On the other hand, when $d \approx w$, $\mathcal{D} \rightarrow 1$, and the Kittel mode is circularly polarized. When $d \lesssim w$, and the Kittel mode traces an elliptical orbit. Figure 1.5 illustrates the chirality of the coupling parameter $g_{\mathbf{k}}$ of the k_z-Kittel mode in a nanowire of dimensions $w = 70$ nm and $d = 20$ nm and magnons in a film of thickness $s = 20$ nm with wave vector $\mathbf{k} = (0, k_y, k_z)$ [8]. The coupling maximum can be shifted to larger momenta by a smaller feature size of the wire. The excitation of such short-wavelength spin waves is possible with a magnetically hard transducer that has a high ferromagnetic resonance frequency [5, 25, 26, 27, 28, 29].
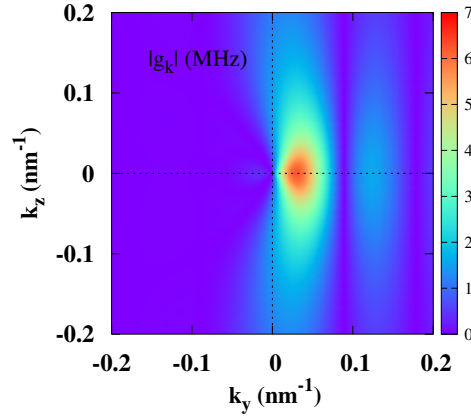

Fig. 1.5 Momentum dependence of the dipolar coupling strength $|g_{\mathbf{k}}|$ of a magnetic nanowire and film (parameters in the text) [8].

1.3.3 Coherent chiral spin wave transmission

The quantum description leads to expressions that are fully equivalent with Eq. (1.21) obtained from the classical description [52, 53]. The excitation of magnons saps nanowire energy and angular momentum, thereby contributing to the magnetization damping, which can be observed as an increased linewidth of the ferromagnetic resonance spectrum. In the quantum description, this broadening is determined by the imaginary part of the magnetic self-energy, which in the first Born approximation or the Fermi-golden rule reads

$$\delta\tilde{\kappa}_{k_z} = 2\pi \sum_{k_y} |g_{\mathbf{k}}|^2 \delta(\tilde{\omega}_{k_z} - \omega_{\mathbf{k}}). \qquad (1.36)$$

We predict a very significant additional damping for a Co nanowire with width $w = 70$ nm, thickness $d = 20$ nm, magnetization $\mu_0\tilde{M}_s = 1.1$ T [7, 29], and exchange stiffness $\tilde{\lambda}_{\text{ex}} = 3.1 \times 10^{-13}$ cm^2 [54]. We adopt a YIG film $s = 20$ nm with magnetization $\mu_0 M_s = 0.177$ T and exchange stiffness $\lambda_{\text{ex}} = 3.0 \times 10^{-12}$ cm^2 [7, 29, 38]. A magnetic field $\mu_0 H_{\text{app}} = 0.05$ T is sufficient to switch the film magnetizations antiparallel to that of the wire to maximize the effect [28, 29]. The calculated additional damping of nanowire Kittel dynamics is then $\delta\alpha_{\text{Co}} = \delta\tilde{\kappa}_{k_z=0}/(2\tilde{\omega}_{k_z=0}) = 3.1 \times 10^{-2}$, which is one order of magnitude larger than the intrinsic Gilbert damping coefficient $\alpha_{\text{Co}} = 2.4 \times 10^{-3}$ [55].

Almost perfect chiral pumping by a nanowire *array* has been observed by the microwave transmission and Brillouin light scattering in Ref. [7]. We here focus on the new features in the broadband non-local excitation-detection by *two nanowires*. The magnetic order in two nanowires located at $\mathbf{r}_1 = R_1\hat{\mathbf{y}}$ and $\mathbf{r}_2 = R_2\hat{\mathbf{y}}$ act as transducers for microwaves that are emitted or absorbed by local microwave (normal metal) antennas such as coplanar wave guides. The observable is the scattering matrix of the microwaves with excitation (input) at R_1 and the detection (output) at R_2, which can be formulated by the input-output theory [52, 53]. The equation of motion of magnons localized at R_1 and R_2 with operators $\hat{m}_L$ and $\hat{m}_R$ and coupled by the film magnons with operators $\hat{\alpha}_q$ (not to be confused with the Gilbert damping constant) read

$$\frac{d\hat{m}_L}{dt} = -i\omega_K\hat{m}_L(t) - i\sum_q g_q e^{iqR_1}\hat{\alpha}_q(t) - \left(\frac{\kappa_L}{2} + \frac{\kappa_{p,L}}{2}\right)\hat{m}_L(t) - \sqrt{\kappa_{p,L}}\hat{p}_{\text{in}}^{(L)}(t),$$

$$\frac{d\hat{m}_R}{dt} = -i\omega_K\hat{m}_R(t) - i\sum_q g_q e^{iqR_2}\hat{\alpha}_q(t) - \frac{\kappa_R}{2}\hat{m}_R(t),$$

$$\frac{d\hat{\alpha}_q}{dt} = -i\omega_q\hat{\alpha}_q(t) - ig_q e^{-iqR_1}\hat{m}_L(t) - ig_q e^{-iqR_2}\hat{m}_R(t) - \frac{\kappa_q}{2}\hat{\alpha}_q(t). \qquad (1.37)$$

Here, κ_L and κ_R are the intrinsic damping of the Kittel modes in the left and right nanowires, respectively, $\kappa_{p,L}$ is the additional radiative damping induced by the microwave photons $\hat{p}_{\text{in}}^{(L)}$, i.e. the coupling of the left nanowire with the microwave source, and κ_q denotes the intrinsic (Gilbert) damping of magnons in the films. In frequency space:

$$\hat{\alpha}_q(\omega) = g_q G_q(\omega)\left[e^{-iqR_1}\hat{m}_L(\omega) + e^{-iqR_2}\hat{m}_R(\omega)\right],$$

$$\hat{m}_R(\omega) = \frac{-i\sum_q g_q^2 G_q(\omega) e^{iq(R_2-R_1)}}{-i(\omega-\omega_K) + \kappa_R/2 + i\sum_q g_q^2 G_q(\omega)}\hat{m}_L(\omega),$$

$$\hat{m}_L(\omega) = \frac{-\sqrt{\kappa_{p,L}}}{-i(\omega-\omega_K) + (\kappa_L+\kappa_{p,L})/2 + i\sum_q g_q^2 G_q(\omega) - f(\omega)}\hat{p}_{\text{in}}^{(L)}(\omega), \quad (1.38)$$

with spin wave propagator $G_q(\omega) = \left[(\omega - \omega_q) + i\kappa_q/2\right]^{-1}$ and

$$f(\omega) \equiv -\frac{\left(\sum_q g_q^2 G_q(\omega) e^{iq(R_1-R_2)}\right)\left(\sum_q g_q^2 G_q(\omega) e^{iq(R_2-R_1)}\right)}{-i(\omega - \omega_K) + \kappa_R/2 + i\sum_q g_q^2 G_q(\omega)}. \qquad (1.39)$$

The excitation of the left nanowire propagates to the right nanowire by the spin waves in the film. When chiral coupling is perfect, $f(\omega)$ vanishes without the back-action. The microwave output of both left and right nanowires as inductively detected by coplanar wave guides are denoted $\hat{p}_{out}^{(L)}(\omega)$ and $\hat{p}_{out}^{(R)}(\omega)$ with input-output relations [52, 53]

$$\hat{p}_{out}^{(L)}(\omega) = p_{in}^{(L)}(\omega) + \sqrt{\kappa_{p,L}}\hat{m}_L(\omega),$$
$$\hat{p}_{out}^{(R)}(\omega) = \sqrt{\kappa_{p,R}}\hat{m}_R(\omega), \qquad (1.40)$$

where $\kappa_{p,R}$ is the additional radiative damping induced by the detector. Therefore, the elements in the microwave scattering matrix describing reflection (S_{11}) and transmission (S_{21}) amplitudes become

$$S_{11}(\omega) \equiv \frac{\hat{p}_{out}^{(L)}}{\hat{p}_{in}^{(L)}} = 1 - \frac{\kappa_{p,L}}{-i(\omega - \omega_K) + (\kappa_L + \kappa_{p,L})/2 + i\sum_q g_q^2 G_q(\omega) - f(\omega)},$$

$$S_{21}(\omega) \equiv \frac{\hat{p}_{out}^{(R)}}{\hat{p}_{in}^{(L)}} = [1 - S_{11}(\omega)]\sqrt{\frac{\kappa_{p,R}}{\kappa_{p,L}}}\frac{i\sum_q g_q^2 G_q(\omega) e^{iq(R_2-R_1)}}{-i(\omega - \omega_K) + \kappa_R/2 + i\sum_q g_q^2 G_q(\omega)}.$$

$$(1.41)$$

The real parts of S_{11} and S_{12} at different magnetic fields and microwave frequencies are illustrated in Fig. 1.6 for antiparallel magnetizations. The frequency of the Co Kittel mode decreases with increasing magnetic field until its direction is reversed to the magnetic-field direction (here $|H_{app}| \lesssim 200$ mT). The interference pattern on the Kittel resonance in Fig. 1.6(b) reflects the transmission phase delay $e^{ik(R_1-R_2)}$ in Eq. (1.41). We note that in our model the nanowires do not reflect spin waves, the features should therefore not be interpreted in terms of standing spin waves.

1.3.4 Incoherent chiral pumping

A temperature gradient between the magnetic nanowire and film also injects unidirectional magnon currents, i.e., causes a chiral spin Seebeck effect [59, 60, 61, 62]. Here we consider again two identical transducers, i.e., a magnetic nanowire at $\mathbf{r}_2 = R_2\hat{\mathbf{y}}$ that detects magnons, which are now thermally injected by the nanowire at $\mathbf{r}_1 = R_1\hat{\mathbf{y}}$ and $R_1 < R_2$. This is the configuration of the non-local spin Seebeck effect as detected electrically in many experiments starting with Ref. [21]. The magnons in those experiments are believed to be injected by the interface exchange interaction
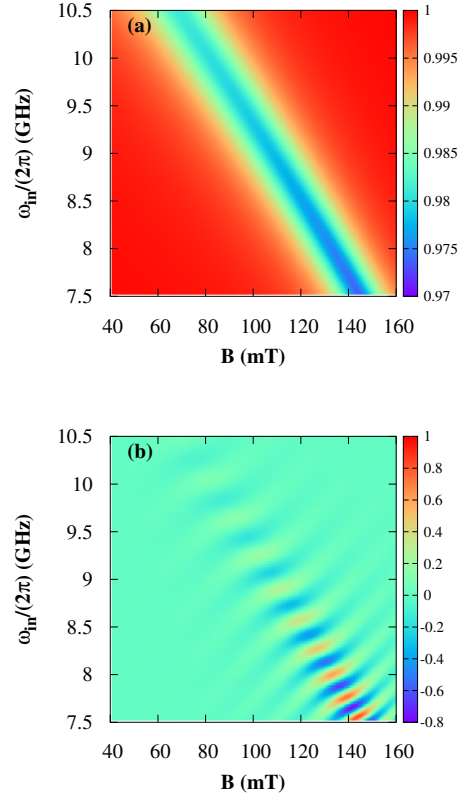
Fig. 1.6 Microwave reflection ReS_{11} [(a)] and transmission ReS_{12} [(b)] amplitudes, Eqs. (1.41), for a system of two Co nanowires on a YIG film as a function of frequency ω_{in}. The radiative damping of both nanowires is $\kappa_p/(2\pi) = 10$ MHz and other parameters are given in the text.

or generated by a temperature gradient in the bulk and results are interpreted by spin diffusion models. Here we consider the regime in which the exchange effect is suppressed, magnon propagation is ballistic and we disregard the bulk spin See-beck effect due to possible temperature gradients. We predict a spin non-local spin Seebeck effect that is caused exclusively by dipolar fields and carried by magnons with long wave lengths and lifetimes. We focus on the Kittel magnons in the wires since the dipolar coupling between the film and higher bands in the nanowire is very small. The coupling strength $|g_{\mathbf{k}}|$ in Fig. 1.5 illustrates that magnons with wavelength around half of the nanowire width (here $\pi/w = 0.045$ nm^{-1}) dominate the coupling. Pumping from other than the those modes can therefore be disregarded even at elevated temperatures. Furthermore, the spin current in the film is dominated by spin waves with small momentum and long mean-free paths, so the effects of magnon-magnon and magnon-phonon interactions that otherwise render magnon transport

phenomena diffuse [21] should be negligibly small. The narrow-band thermal injection requires an inductive (or optical) detection of the magnons accumulated in the detector contact, since the inverse spin Hall effect with heavy metal contacts is very inefficient.

The equation of motions of the Kittel modes in the nanowire and film spin waves with momentum q in the coupled system read

$$\frac{d\hat{m}_L}{dt} = -i\omega_K \hat{m}_L - \sum_q ig_q^* e^{iqR_1}\hat{\alpha}_q - \frac{\kappa}{2}\hat{m}_L - \sqrt{\kappa}\hat{N}_L,$$

$$\frac{d\hat{m}_R}{dt} = -i\omega_K \hat{m}_R - \sum_q ig_q^* e^{iqR_2}\hat{\alpha}_q - \frac{\kappa}{2}\hat{m}_R - \sqrt{\kappa}\hat{N}_R,$$

$$\frac{d\hat{\alpha}_q}{dt} = -i\omega_q \hat{\alpha}_q - ig_q e^{-iqR_1}\hat{m}_L - ig_q e^{-iqR_2}\hat{m}_R - \frac{\kappa_q}{2}\hat{\alpha}_q - \sqrt{\kappa_q}\hat{N}_q, \qquad (1.42)$$

where κ is caused by the same Gilbert damping in both nanowires, and $\hat{N}_L$ and $\hat{N}_R$ represent the thermal noise in the left and right nanowires, with $\langle \hat{N}_\eta^\dagger(t)\hat{N}_{\eta'}(t') \rangle = n_\eta \delta(t-t')\delta_{\eta\eta'}$. Here, $\eta \in \{L, R\}$ and $n_\eta = 1/\{\exp\left[\hbar\tilde{\omega}_K/(k_B T_\eta)\right] - 1\}$ and T_R is also the film temperature. Integrating out the spin-wave modes in the film, we obtain equations for dissipatively coupled [63, 64] nanowires. In frequency space,

$$\left(-i(\omega - \omega_K) + \frac{\kappa}{2} + \frac{\Gamma_1 + \Gamma_2}{2}\right)\hat{m}_L(\omega) + \Gamma_2 e^{iq_*|R_2 - R_1|}\hat{m}_R(\omega) \qquad (1.43)$$

$$= \sum_q ig_q^* e^{iqR_1}\sqrt{\kappa_q}G_q(\omega)\hat{N}_q(\omega) - \sqrt{\kappa}\hat{N}_L(\omega),$$

$$\left(-i(\omega - \omega_K) + \frac{\kappa}{2} + \frac{\Gamma_1 + \Gamma_2}{2}\right)\hat{m}_R(\omega) + \Gamma_1 e^{iq_*|R_2 - R_1|}\hat{m}_L(\omega)$$

$$= \sum_q ig_q^* e^{iqR_2}\sqrt{\kappa_q}G_q(\omega)\hat{N}_q(\omega) - \sqrt{\kappa}\hat{N}_R(\omega), \qquad (1.44)$$

where $\Gamma_1 = |g_{q_*}|^2/v_{q_*}$ and $\Gamma_2 = |g_{-q_*}|^2/v_{q_*}$ are assumed constant (for the Kittel mode). Here, q_* is the positive root of $\omega_{q_*} = \tilde{\omega}_K$.

For perfectly chiral coupling with $\Gamma_2 = 0$ the solutions of Eqs. (1.44) read

$$\hat{m}_L(\omega) = \frac{\sum_q ig_q^* e^{iqR_1}\sqrt{\kappa_q}G_q(\omega)\hat{N}_q(\omega) - \sqrt{\kappa}\hat{N}_L(\omega)}{-i(\omega - \omega_K) + \frac{\kappa}{2} + \frac{\Gamma_1}{2}},$$

$$\hat{m}_R(\omega) = \frac{\sum_q ig_q^* e^{iqR_2}\sqrt{\kappa_q}G_q(\omega)\hat{N}_q(\omega) - \sqrt{\kappa}\hat{N}_R(\omega) - \Gamma_1 e^{q_*(R_2 - R_1)}\hat{m}_L(\omega)}{-i(\omega - \omega_K) + \frac{\kappa}{2} + \frac{\Gamma_1}{2}}.$$

$$(1.45)$$

With $\hat{m}_{L,R}(t) = \int e^{-i\omega t}\hat{m}_{L,R}(\omega)d\omega/(2\pi)$, the Kittel modes are occupied according to

$$\rho_L \equiv \langle \hat{m}_L^\dagger(t)\hat{m}_L(t)\rangle = n_L + \int \frac{d\omega}{2\pi} \frac{\kappa}{(\omega - \omega_K)^2 + (\kappa/2 + \Gamma_1/2)^2}(n_{q_*} - n_L),$$

(1.46)

$$\rho_R \equiv \langle \hat{m}_R^\dagger(t)\hat{m}_R(t)\rangle = n_R + \int \frac{d\omega}{2\pi} \frac{\Gamma_1^2 \kappa}{\left[(\omega - \omega_K)^2 + (\kappa/2 + \Gamma_1/2)^2\right]^2}(n_L - n_{q_*}),$$

(1.47)

where the damping in the high-quality film has been disregarded $(\kappa_q \to 0)$. In the linear regime the non-local thermal injection of magnons into the right transducer by the left one then reads

$$\delta\rho_R = \begin{cases} S_{\text{CSSE}}(T_L - T_R) \\ 0 \end{cases} \text{when} \begin{array}{l} T_L > T_R \\ T_L \leq T_R \end{array},$$

$$S_{\text{CSSE}} = \int \frac{d\omega}{2\pi} \frac{\Gamma_1^2 \kappa}{\left[(\omega - \omega_K)^2 + (\kappa/2 + \Gamma_1/2)^2\right]^2} \left.\frac{dn_L}{dT}\right|_{T=(T_L+T_R)/2}.$$

(1.48)

where we defined the chiral (or dipolar) spin Seebeck coefficient S_{CSSE}.

The device therefore operates as a heat diode, apparently acting as a "Maxwell demon" that rectifies the thermal fluctuations at equilibrium. However, in thermal equilibrium all right and left moving magnons are eventually connected by reflection of spin waves at the edges and absorption and re-emission by connected heat baths. The Second Law of thermodynamics is therefore safe, but it might be interesting to search for chirality-induced transient effects.

1.4 Conclusion and outlook

Handedness or chirality of wave propagation is a popular research topic in optics, acoustics, and condensed matter physics. Here we contribute by a theory for the coherent and incoherent chiral pumping of spin waves into thin magnetic films through the chiral magnetodipolar radiation generated by the Oersted field of metallic striplines and dipolar field of magnetic nanostructures. Spin waves excited coherently in the film under magnetic resonance of the nanowire are unidirectional, generating a non-equilibrium magnetization in only half of the film. A temperature gradient between a local magnet and a film leads to the unidirectional excitation of incoherent magnons, i.e., a chiral spin Seebeck effect.

$\mathcal{PT}$ symmetry has been predicted to amplify unidirectional response [56, 57, 58]. Even though our system is dissipative and therefore not PT symmetric, the nonreciprocal coupling of the two wires still allows directional amplification [9, 10]. It would be interesting to introduce $\mathcal{PT}$ symmetry into our system via gain in one wire that compensates the damping in the other, possibly leading to enhanced effects.

Magnons can interact remotely by their chiral dipolar magnetic fields with other quasiparticles including other magnons, photons, phonons, and conduction electron spins. Strong chiral coupling between magnons and photons exist, e.g., in microwave waveguides or cavities that contain chains of small magnets on special lines [9, 10]. Large magnon numbers accumulate at one edge of a chain of magnets when excited by local antennas [9, 10]. Spin currents by electrons or phonons may be generated by the chiral magnetodipolar radiation as well. Chirality is a functionality that has not yet been employed much in spintronics, but could be the basis for a new generation of spin-based devices made from conventional materials.

References

1. B. Lenk, H. Ulrichs, F. Garbs, and M. Muenzenberg, Phys. Rep. **507**, 107 (2011).
2. A. V. Chumak, V. I. Vasyuchka, A. A. Serga, and B. Hillebrands, Nat. Phys. **11**, 453 (2015).
3. D. Grundler, Nat. Nanotechnol. **11**, 407 (2016).
4. V. E. Demidov, S. Urazhdin, G. de Loubens, O. Klein, V. Cros, A. Anane, and S. O. Demokritov, Phys. Rep. **673**, 1 (2017).
5. Y. Au, E. Ahmad, O. Dmytriiev, M. Dvornik, T. Davison, and V. V. Kruglyak, Appl. Phys. Lett. **100**, 182404 (2012).
6. T. Yu, C. P. Liu, H. M. Yu, Y. M. Blanter, and G. E. W. Bauer, Phys. Rev. B **99**, 134424 (2019).
7. J. L. Chen, T. Yu, C. P. Liu, T. Liu, M. Madami, K. Shen, J. Y. Zhang, S. Tu, M. S. Alam, K. Xia, M. Z. Wu, G. Gubbiotti, Y. M. Blanter, G. E. W. Bauer, and H. M. Yu, Phys. Rev. B **100**, 104427 (2019).
8. T. Yu, Y. M. Blanter, and G. E. W. Bauer, Phys. Rev. Lett. **123**, 247202 (2019).
9. T. Yu, Y.-X. Zhang, S. Sharma, Y. M. Blanter, and G. E. W. Bauer, Phys. Rev. Lett. **124**, 107202 (2020).
10. T. Yu, X. Zhang, S. Sharma, Y. M. Blanter, and G. E. W. Bauer, Phys. Rev. B **101**, 094414 (2020).
11. P. Lodahl, S. Mahmoodian, S. Stobbe, A. Rauschenbeutel, P. Schneeweiss, J. Volz, H. Pichler, and P. Zoller, Nature (London) **541**, 473 (2017).
12. F. Le Kien, S. D. Gupta, K. P. Nayak, and K. Hakuta, Phys. Rev. A **72**, 063815 (2005).
13. M. Scheucher, A. Hilico, E. Will, J. Volz, and A. Rauschenbeutel, Science **354**, 1577 (2016).
14. P. Lodahl, S. Mahmoodian, S. Stobbe, A. Rauschenbeutel, P. Schneeweiss, J. Volz, H. Pichler, and P. Zoller, Nature **541**, 473 (2017).
15. B. Vermersch, P.-O. Guimond, H. Pichler, and P. Zoller, Phys. Rev. Lett. **118**, 133601 (2017).
16. P. Schneeweiss, S. Zeiger, T. Hoinkes, A. Rauschenbeutel, and J. Volz, Opt. Lett. **42**, 85 (2017).
17. C. A. Downing, J. C. López Carreño, F. P. Laussy, E. del Valle, and A. I. Fernández-Domínguez, Phys. Rev. Lett. **122**, 057401 (2019).
18. F. J. Rodríguez-Fortuño, G. Marino, P. Ginzburg, D. O'Connor, A. Martínez, G. A. Wurtz, and A. V. Zayats, Science **340**, 328 (2013).
19. J. Petersen, J. Volz, and A. Rauschenbeutel, Science **346**, 67 (2014).
20. H. Chang, P. Li, W. Zhang, T. Liu, A. Hoffmann, L. Deng, and M. Wu, IEEE Magn. Lett. **5**, 6700104 (2014).

21. L. J. Cornelissen, J. Liu, R. A. Duine, J. Ben Youssef, and B. J. van Wees, Nat. Phys. **11**, 1022 (2015).

22. K. Uchida, H. Adachi, T. An, T. Ota, M. Toda, B. Hillebrands, S. Maekawa, and E. Saitoh, Nature Mater. **10**, 737 (2011).

23. A. A. Serga, A. V. Chumak, and B. Hillebrands, J. Phys. D **43**, 264002 (2010).

24. *Nanomagnetism and Spintronics*, edited by T. Shinjo (Elsevier, Oxford, 2009).

25. H. Yu, G. Duerr, R. Huber, M. Bahr, T. Schwarze, F. Brandl, and D. Grundler, Nat. Commun. **4**, 2702 (2013).

26. H. Qin, S. J. Hämäläinen, and S. van Dijken, Sci. Rep. **8**, 5755 (2018).

27. S. Klingler, V. Amin, S. Geprägs, K. Ganzhorn, H. Maier-Flaig, M. Althammer, H. Huebl, R. Gross, R. D. McMichael, M. D. Stiles, S. T. B. Goennenwein, and M. Weiler, Phys. Rev. Lett. **120**, 127201 (2018).

28. C. P. Liu, J. L. Chen, T. Liu, F. Heimbach, H. M. Yu, Y. Xiao, J. F. Hu, M. C. Liu, H. C. Chang, T. Stueckler, S. Tu, Y. G. Zhang, Y. Zhang, P. Gao, Z. M. Liao, D. P. Yu, K. Xia, N. Lei, W. S. Zhao, and M. Z. Wu, Nat. Commun. **9**, 738 (2018).

29. J. L. Chen, C. P. Liu, T. Liu, Y. Xiao, K. Xia, G. E. W. Bauer, M. Z. Wu, and H. M. Yu, Phys. Rev. Lett. **120**, 217202 (2018).

30. L. R. Walker, Phys. Rev. **105**, 390 (1957).

31. R. W. Damon and J. R. Eshbach, J. Phys. Chem. Solids **19**, 308 (1961).

32. A. Akhiezer, V. Baríakhtar, and S. Peletminski, *Spin Waves* (North-Holland, Amsterdam, 1968).

33. D. D. Stancil and A. Prabhakar, *Spin Waves–Theory and Applications* (Springer, New York, 2009).

34. T. An, V. I. Vasyuchka, K. Uchida, A. V. Chumak, K. Yamaguchi, K. Harii, J. Ohe, M. B. Jungfleisch, Y. Kajiwara, H. Adachi, B. Hillebrands, S.Maekawa, and E. Saitoh, Nat. Mater. **12**, 549 (2013).

35. O. Wid, J. Bauer, A. Müller, O. Breitenstein, S. S. P. Parkin, and G. Schmidt, Sci. Rep. **6**, 28233 (2016).

36. E. Shigematsu, Y. Ando, S. Dushenko, T. Shinjo, and M. Shiraishi, Appl. Phys. Lett. **112**, 212401 (2018).

37. P. Wang, L. F. Zhou, S. W. Jiang, Z. Z. Luan, D. J. Shu, H. F. Ding, and D. Wu, Phys. Rev. Lett. **120**, 047201 (2018).

38. T. Yu, S. Sharma, Y. M. Blanter, and G. E. W. Bauer, Phys. Rev. B **99**, 174402 (2019).

39. I. Bertelli, J. J. Carmiggelt, T. Yu, B. G. Simon, C. C. Pothoven, G. E. W. Bauer, Y. M. Blanter, J. Aarts, and T. van der Sar, arXiv:2004.07746.

40. H. C. Wang, J. L. Chen, T. Yu, C. P. Liu, C. Y. Guo, H. Jia, S. Liu, K. Shen, T. Liu, J. Y. Zhang, M. A. C. Z, Q. M. Song, S. Tu, M. Z. Wu, X. F. Han, K. Xia, D. P. Yu, G. E. W. Bauer, and H. M. Yu, arXiv:2005.10452.

41. L. Novotny and B. Hecht, *Principles of Nano-Optics* (Cambridge University Press, Cambridge, England, 2006).

42. J. D. Jackson, *Classical Electrodynamics*, (Wiley, New York, 1998).

43. T. Schneider, A. A. Serga, T. Neumann, B. Hillebrands, and M. P. Kostylev, Phys Rev B **77**, 214411 (2008).

44. V. E. Demidov, M. P. Kostylev, K. Rott, P. Krzysteczko, G. Reiss, and S. O. Demokritov, Appl. Phys. Lett, **95**, 2509 (2009).

45. C. Kittel, *Quantum Theory of Solids* (Wiley, New York, 1963).

46. T. Holstein and H. Primakoff, Phys. Rev. **58**, 1098 (1940).

47. L. D. Landau and E. M. Lifshitz, *Electrodynamics of Continuous Media*, 2nd ed. (Butterworth-Heinenann, Oxford, 1984).

48. G. D. Mahan, *Many Particle Physics* (Plenum, New York, 1990).

49. M. Büttiker, H. Thomas, and A. Prêtre, Z. Phys. B **94**, 133 (1994).

50. Y. Tserkovnyak, A. Brataas, and G. E. W. Bauer, Phys. Rev. Lett. **88**, 117601 (2002).

51. Y. Tserkovnyak, A. Brataas, G. E. W. Bauer, and B. I. Halperin, Rev. Mod. Phys., **77**, 1375 (2005).

52. C. W. Gardiner and M. J. Collett, Phys. Rev. A **31**, 3761 (1985).
53. A. A. Clerk, M. H. Devoret, S. M. Girvin, F. Marquardt, and R. J. Schoelkopf, Rev. Mod. Phys. **82**, 1155 (2010).
54. R. Moreno, R. F. L. Evans, S. Khmelevskyi, M. C. Muñoz, R. W. Chantrell, and O. Chubykalo-Fesenko, Phys. Rev. B **94**, 104433 (2016).
55. M. A. W. Schoen, D. Thonig, M. L. Schneider, T. J. Silva, H. T. Nembach, O. Eriksson, O. Karis, and J. M. Shaw, Nat. Phys. **12**, 839 (2016).
56. A. Mostafazadeh, J. Phys. A: Math. Theor. **47**, 505303 (2014).
57. L. Ge, Y. D. Chong, and A. D. Stone, Phys. Rev. A **85**, 023802 (2012).
58. A. Galda and V. M. Vinokur, Phys. Rev. B **94**, 020408(R) (2016).
59. K. Uchida, J. Xiao, H. Adachi, J. Ohe, S. Takahashi, J. Ieda, T. Ota, Y. Kajiwara, H. Umezawa, H. Kawai, G. E. W. Bauer, S. Maekawa, and E. Saitoh, Nat. Mater. **9**, 894 (2010).
60. J. Xiao, G. E. W. Bauer, K. Uchida, E. Saitoh, and S. Maekawa, Phys. Rev. B **81**, 214418 (2010).
61. H. Adachi, J. Ohe, S. Takahashi, and S. Maekawa, Phys. Rev. B **83**, 094410 (2011).
62. G. E. W. Bauer, E. Saitoh, and B. J. van Wees, Nat. Mat. **11**, 391 (2012).
63. B. M. Yao, T. Yu, X. Zhang, W. Lu, Y. S. Gui, C.-M. Hu, and Y. M. Blanter, Phys. Rev. B **100**, 214426 (2019).
64. B. M. Yao, T. Yu, Y. S. Gui, J. W. Rao, Y. T. Zhao, W. Lu, and C.-M. Hu, Commun. Phys. **2**, 161 (2019).